16_5_01

by Willyanto A

Submission date: 02-Nov-2021 09:05AM (UTC+0700)
Submission ID: 1690585006
File name: 16_5_01.pdf (2.94M)
Word count: 8159
Character count: 40567

Journal of Engineering Science and Technology
Vol. 16, No. 5 (2021) 3600 – 3619

EFFECTS OF INTAKE FLOW ON IN-CYLINDER SWIRL FLOW UNDER MOTORING AND FIRING CONDITIONS FOR CI ENGINES USING PIV MEASUREMENTS

M. ICHIYANAGI[1], R. SAITO[1], Y. SAWAMURA[1], G. NDIZEYE[1], G. J. GOTAMA[2, 3], W. ANGGONO[4, 5, *], T. SUZUKI[1]

[1]Department of Engineering and Applied Sciences, Sophia University, 7-1 Kioi-cho, Chiyoda-ku, Tokyo 102-8554, Japan
[2]School of Mechanical and Aerospace Engineering, Nanyang Technological University, 50 Nanyang Avenue, 639798 Singapore
[3]Department of Aerospace and Geodesy, Technical University of Munich, Willy-Messerschmitt-Str. 1, Taufkirchen/Ottobrunn 82024, Germany
[4]Mechanical Engineering Department, Petra Christian University, Jalan Siwalankerto No. 121-131, Surabaya, Jawa Timur 60236, Indonesia
[5]Centre for Sustainable Energy Studies, Petra Christian University, Jalan Siwalankerto No. 121-131, Surabaya, Jawa Timur 60236, Indonesia
*Corresponding Author: willy@petra.ac.id

Abstract

The in-cylinder flow during intake and compression strokes in engines significantly affects the fuel-air mixing, combustion, and emissions. In this study, the in-cylinder swirl flow velocities in an optical single-cylinder combustion ignition (CI) engine were measured using particle image velocimetry (PIV) under various driving conditions. As a result, comparing motoring and firing, the flow structures for expansion and exhaust strokes differed but almost resembled for intake and compression strokes. To evaluate the intake and compression strokes, the flow velocities under motoring conditions were used. Comparing the maximum velocity under different engine speeds, it was found that the flow structure did not change significantly, but the flow velocity increased as the engine speed increased. The swirl centre position varied at each crank angle and showed a counter-clockwise trajectory, and the centre positions differed at each plane. These results indicate that different flow structures could be confirmed by changing the measurement plane. Furthermore, comparing the swirl ratio at a different helical port opening ratio, the swirl ratio increased as the opening ratio decreased. It suggested that the intake air from the helical port disturbed the large vortex structure and caused the swirl ratio to decrease. Additionally, comparing the swirl ratio when the measurement plane and intake port opening ratio were changed simultaneously, the order of in-cylinder average variance was Tan., 1/3 Heli., 1/2 Heli., and Double. When comparing the distance between the swirl centre and cylinder centre, and turbulent kinetic energy, it showed the same tendency as the swirl ratio.

Keywords: Helical port, Particle image velocimetry, Swirl flow, Tangential port, Turbulent kinetic energy.

1. Introduction

In the automotive industry, fuel efficiency and exhaust gas emission regulations for internal combustion (IC) engines are becoming more severe year by year [1] due to environmental issues such as global warming, and thus, the use of renewable fuels [2, 3], as well as improvement of engine performance [4], are indispensable. As diesel engines have a higher thermal efficiency [5, 6] and less carbon dioxide (CO_2) emissions than those of gasoline engines, they have been attracting attention. Proper fuel-air mixing in a diesel engine leads to better combustion and emissions performances, and the in-cylinder flow significantly affects the fuel-air mixing [7]. Therefore, the measurement and analysis of in-cylinder flow are crucial, and several past studies have been conducted. Yilmaz et al. [8] studied the intake flow parameters such as mass flow and temperature that affect the overall efficiency of the engine. Furthermore, early work by Takahashi et al. [9] employed laser doppler velocimetry (LDV) to measure the in-cylinder flow; however, although the time and spatial resolution are good, the spatial structure cannot be observed instantly. In regard to the flow field inside the cylinder of an engine, it is important to understand the flow for the whole surface.

In combustion ignition (CI) engines, the swirl flow may be generated using the helical port [10]. The swirl flow governs the general speed and direction of the mainstream, and therefore much research has been done about the swirl flow. Since the characteristics of the swirl flow are governed by many experimental conditions including the engine speed and the intake port, it is necessary to understand the flow structure by varying the experimental conditions. Several previous studies clarified the in-cylinder flow by measuring the swirl flow under various experimental conditions using particle image velocimetry (PIV). Heim et al. [11] measured the swirl flow at multiple engine speeds, which clarified that the swirl ratio and the swirl centre position were almost the same even when the engine speed was changed. Kim et al. [12] evaluated the swirl ratio of the swirl flow, which was controlled by changing the opening condition of the intake port. The results showed that closing one of the two intake ports increased the swirl ratio. However, few studies have evaluated the effect of the opening area of the intake port on the swirl centre and the three-dimensional swirl centre position. On the other hand, Okura et al. [13] calculated the turbulence intensity and turbulent kinetic energy, which indicated the magnitude of the turbulence of the flow. However, the in-cylinder flow turbulence was evaluated only near the spark plug because experiments were conducted using a spark ignition (SI) engine. For a CI engine, the in-cylinder flow in the entire combustion chamber must be considered due to the diffusion type of combustion.

With the importance of understanding the intake flow of cylindrical engines [14], this study aims to investigate the in-cylinder gas flow velocities in an optical single-cylinder diesel engine using a PIV system. Using the obtained velocity data, the swirl ratio, turbulent kinetic energy, and the centre position of the swirl flow were analysed during each stroke. The flow velocities were evaluated under different driving conditions such as motoring and firing, different engine speeds of 1000 rpm, 1200 rpm, 1500 rpm, different measurement planes of 40 mm, 60 mm, 80 mm from the cylinder head, and different opening ratios for each intake port. Furthermore, the flow velocities were evaluated when the measurement plane and the intake port opening ratio were changed simultaneously.

2. Experimental Apparatus and Evaluation Technique

2.1. Experimental apparatus and conditions

Tables 1 and 2 show the engine specifications and the PIV system configurations, respectively. In the present study, the schematic diagram of the experimental setup, ports location and *xyz* coordinates are shown in Fig. 1 and the experimental conditions are listed in Table 3. A similar setup has been used in the previous study [15]. The cylinder liner and the piston cavity were made of the fused silica glass and sapphire glass, respectively; enabling to visualize inside the cylinder from the side and the bottom. The gas flow velocity was measured by injecting silicon dioxide (SiO_2) particles of an average diameter of approximately 4.65 µm inside the cylinder. An Nd:YAG laser of a 532 nm wavelength was used with a combination of an optical system to pass a laser sheet of 1 mm thick through the cylinder, to form a 2-D measurement plane. The engine's rotary encoder signal at every crank angle was sent to the high-speed complementary metal-oxide semiconductor (CMOS) camera and the pulse generator. The camera was configured to receive the signal only once every two times and capture two frames with a short time interval per signal. The experiment was carried out under the conditions of the engine speed of 1000 rpm, 1200 rpm, and 1500 rpm and the naturally aspirated air intake. Since the crank angle (CA) signal from the engine is synchronized with the camera, when changing the engine speed, the time resolution is changed as well. With the above engine speeds, the instantaneous velocity of gas flow was measured at each CA 2 deg. with a 3.0 kHz, 3.6 kHz, and 4.5 kHz time resolution, respectively. To clarify the effects of the two intake ports (the helical port and the tangential port) on the flow, the opening conditions of the intake port were set to five conditions: only opening the helical port, only opening the tangential port, and changing the opening ratio of the helical port to one-third, one-half, and both ports fully open. The crank angles are defined as after top dead centre (ATDC), and CA 0 deg. is the top dead center (TDC) of the intake stroke.

Table 1. Engine specifications.

Parameters	Unit	Description
Engine	[-]	Single-cylinder diesel engine
Intake ports	[-]	Helical port and tangential port
Number of valves	[-]	4
Bore	[mm]	85.0
Stroke	[mm]	96.9
Compression ratio	[-]	16.3
Cavity diameter	[mm]	51.6

Table 2. PIV system configurations.

Parameters	Description
Laser type	Continuum, Mesa-PIV
Laser pulse type	Nd: YAG, (532 nm), Double Pulse
Laser pulse width	<150 ns
Laser pulse energy	18 MJ
Optical cylindrical lens type	SIGMAKOKI
Optical focal length	1000 mm, 400 mm, -50 mm
High-speed camera type	Photron, FASTCAM SA5
High-speed camera time resolution	15 kHz
High-speed camera spatial resolution	696×704 pixels
Pulse generator	FLOWTECH RESEARCH, VSD2000
Tracer particle seeder type	PIVTEC GmbH
Particles used	SiO_2 particles (4.65 µm)
Air compressor	EARTH MAN, ACP-25SLA

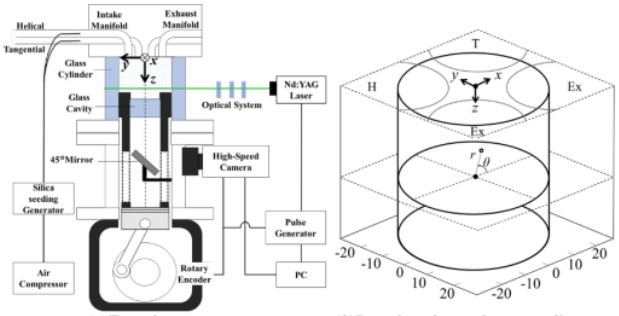

(*a*)Experiment setup (*b*)Ports location and *xyz* coordinates

Fig. 1. Schematic diagram of the experimental setup.

Table 3. PIV experimental conditions.

Parameters	Unit	Description
Engine speed	[rpm]	1000, 1200, 1500
Shooting interval	[μs]	20 (1 pair image / 2 deg.)
Measurement planes	[mm]	z = 40, 60, 80 (Bottom of cylinder head is z = 0)
Intake port conditions	[-]	Helical (Heli.), Tangential (Tan.), 1/3 Helical + Tangential (1/3 Heli.) 1/2 Helical + Tangential (1/2 Heli.) Helical + Tangential (Double)
Fuel quantity	[mg]	4.2
Fuel injection pressure	[MPa]	80
Fuel injection timing	[-]	1 deg. before top dead centre (BTDC)

2.2. Evaluation technique of swirl ratio

The swirl ratio, S_R, is a parameter that indicates the relative strength of a swirl flow inside the cylinder. S_R is calculated by taking the ratio of the average angular velocities in x and y directions which is described in Fig. 1(b), to the engine angular velocity. In the present study, the swirl ratios were calculated using the PIV measurements as follows, [14]

$$S_R = \frac{1}{\omega_{engine}} \times \frac{1}{N} \sum_{i=1}^{N} \frac{v_{i,j} \cdot \cos\theta - u_{i,j} \cdot \sin\theta}{r_{i,j}} \quad (1)$$

where ω_{engine} is the engine angular velocity [rad/s], $r_{i,j}$ is the distance between the cylinder centre and any lattice point [m], θ is the angle of the cylinder centre and any lattice point [rad], N is the total number of lattice points in an entire measurement plane [-], $u_{i,j}$ and $v_{i,j}$ are the velocities in x and y directions [mm/s], respectively. In addition, $r_{i,j}$ and θ are described in Fig. 1(b).

In the present study, using the PIV measurements two kinds of swirl ratios were calculated; one using the centre position of a cylinder as the centre of the swirl flow (referred to as cylinder centre) and the other using the centre position of the swirl flow vortex obtained from the evaluation technique as described in the next section (swirl centre).

2.3. Evaluation technique of swirl centre

The swirl centre obtained using the PIV measurements was identified using the algorithm with a dimensionless scalar gamma function as shown in equation (2) [16], where -1 ≤ Γ ≤ 1.

$$\Gamma(P_{i,j}) = \frac{1}{N}\sum_{l=1}^{N} sin(\theta_l) \quad (2)$$

For any fixed arbitrary lattice point, $P_{i,j}$, in an in-plane velocity field, the function presents the average sine of the angle, θ, between the vectors connecting the point to all other interrogation window centres and those to the measured velocities. The swirl centre is determined as the lattice point with the absolute value of Γ close to 1, which means θ for each integration window would be approximately 90°.

2.4. Evaluation technique of turbulent kinetic energy

The turbulent kinetic energy, k, is a parameter that indicates the strength of turbulence of a flow, which is the magnitude of deviation from the average flow velocity. In the present study, the turbulent kinetic energy was calculated using the PIV measurements as shown in equation (3) [14],

$$k = \frac{1}{N}\sum_{l=1}^{N} \frac{(u'^2+v'^2)}{2} \quad (3)$$

where u' and v' are the turbulent flow velocities in x and y directions, respectively. The turbulent flow velocity is obtained by subtracting the ensemble average velocity from the instantaneous velocity. Turbulent kinetic energy can be used to evaluate the degree of turbulence. For example, when the deviation from the average flow velocity is large, k becomes large, so that it can be evaluated that the mixing action with the surrounding fluid is large.

3. Results and Discussion

3.1. Comparison between motoring and firing conditions

Figure 2 shows the ensemble-averaged velocity-vector maps for in-cylinder gas flow at z = 60 mm from the bottom of the cylinder head under the motoring and the firing conditions. The experiments were conducted under the conditions listed in Table 3, and the representative results for motoring condition at the (a) intake, (b) compression, (c) expansion and (d) exhaust strokes, for firing condition at the (e) intake, (f) compression, (g) expansion and (h) exhaust strokes are shown in each figure. The white dots in the figures represent the identified swirl centre. Observing from the swirl centres, the swirl flow towards the counter-clockwise direction could be formed during all strokes. Additionally, Table 4 shows the coordinates for the maximum velocity and the swirl centre position for each stroke under motoring and the firing conditions, respectively.

Comparing the maximum velocities under motoring and firing conditions, as shown in Table 4, it was found that during the intake, compression, and expansion stroke, the velocity values resembled. However, the maximum flow velocities for the exhaust stroke did not resemble under motoring and firing conditions. Comparing the swirl centre positions from Table 4, for the intake and compression strokes, it was observed that the positions under motoring condition resembled

those under firing condition, respectively. However, during the expansion and exhaust strokes, the swirl centre positions under motoring condition were far to those under firing condition, respectively. From the above, when comparing the maximum flow velocity and the swirl centre position, the flow structures for expansion and exhaust strokes differed but almost resembled for intake and compression strokes. In this study, to evaluate the intake and compression strokes, the comparison for other experimental conditions uses the flow velocity under motoring conditions.

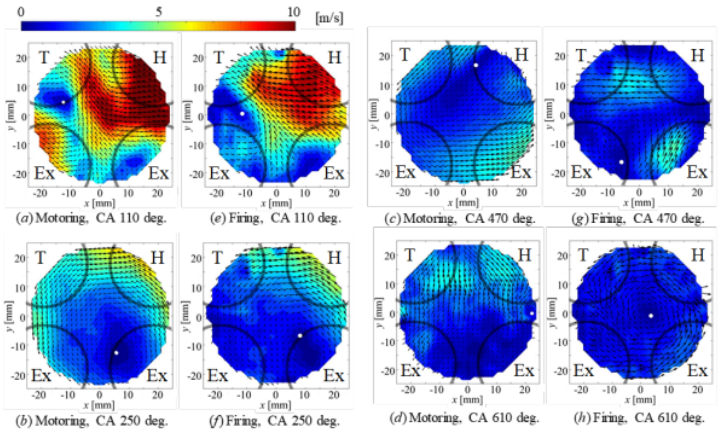

Fig. 2. Ensemble-averaged velocity-vector maps at z = 60 mm under motoring condition for (a) intake, (b) compression, (c) expansion and (d) exhaust stroke, and firing condition for (e) intake, (f) compression, (g) expansion and (h) exhaust stroke.

Table 4. Swirl centre positions and maximum velocities for each stroke under motoring and the firing conditions.

Condition	Maximum velocity [m/s]		Swirl centre position [mm]	
	Motoring	Firing	Motoring	Firing
Intake	12.6	11.0	(-13.4, 4.6)	(-10.3, 0.6)
Compression	7.1	6.2	(5.6, -12.7)	(7.0, -6.3)
Expansion	4.6	4.8	(3.9, 16.7)	(-6.1, -15.9)
Exhaust	4.4	2.6	(22.9, -0.6)	(3.6, -1.1)

3.2. Comparison between different engine speeds

Figure 3 shows the ensemble-averaged velocity-vector maps for in-cylinder gas flow at z = 60 mm under the motoring conditions at 1000, 1200, 1500 rpm. The representative results at the (a) 1000 rpm intake, (b) 1000 rpm compression, (c) 1200 rpm intake, (d) 1200 rpm compression, (e) 1500 rpm intake, (f) 1500 rpm compression stroke are shown in each figure.

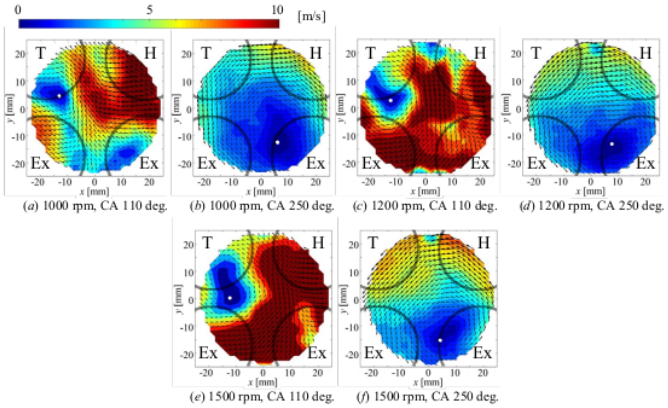

Fig. 3. Ensemble-averaged velocity-vector maps at z = 60 mm for (a) 1000 rpm intake, (b) 1000 rpm compression, (c) 1200 rpm intake, (d) 1200 rpm compression, (e) 1500 rpm intake, and (f) 1500 rpm compression stroke.

Comparing the velocity-vector maps at the same crank angle, it shows that the flow structures were very similar. The swirl centre positions during the intake stroke under 1000 rpm was (x, y) = (-13.4, 4.6), with 1200 and 1500 rpm having swirl centre of (x, y) = (-12.2, 3.1), (x, y) = (-12.1, 0.2), respectively. Similarly, the swirl centre positions during the compression stroke under 1000 rpm were (x, y) = (5.6, -12.7), with 1200 and 1500 rpm having swirl centre of (x, y) = (6.8, -12.5), (x, y) = (5.6, -12.7), respectively. On the other hand, different results were obtained by comparing the maximum velocities. In Table 5, the maximum velocity, and the dimensionless velocity, which is a value obtained by nondimensionalization of the maximum flow rates using the representative speed calculated from the engine speed, are shown for intake and compression strokes. Comparing the velocity, it was found that the velocity increases as the engine speed increases, however, it shows a similar value at any engine speed by making it dimensionless. From these results, it is considered that the change of the engine speed changes the velocity of the flow, though it does not affect the flow structure.

Figure 4 shows the swirl ratio which was calculated from the swirl centre at each engine speed. Under all conditions, the trend resembled, and it is considered that the flow velocity increased in proportion to the engine speed. Furthermore, under all conditions, the maximum swirl ratio is obtained during the intake stroke, and the value decreases as approaching bottom dead centre (BDC) and increases during the compression stroke. The correlation coefficient of the swirl ratio under each condition was 0.94 for 1000 rpm-1200 rpm, 0.93 for 1000 rpm-1500 rpm, and 0.90 for 1200 rpm-1500 rpm. From these results, it was found that the swirl ratio under each condition had a strong correlation. That is, though the swirl ratio changed with a change in crank angles, it was almost the same even when the engine speed changed.

Table 5. Maximum and dimensionless velocities for each stroke under different engine speeds.

Condition	Maximum velocity [m/s]			Dimensionless velocity [-]		
	1000 rpm	1200 rpm	1500 rpm	1000 rpm	1200 rpm	1500 rpm
Intake	12.6	17.6	22.5	3.9	4.5	4.6
Compression	7.1	6.6	8.4	2.2	1.7	1.7

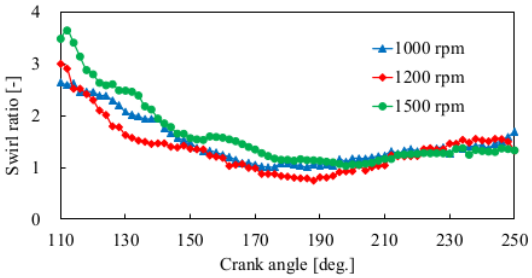

Fig. 4. Comparison of the time evolution of the swirl ratio under different engine speeds.

Figure 5 shows the distance between the swirl centre and the cylinder centre at each crank angle when the engine speed was varied. It was found that the trajectory around the swirl centre shows the same tendency at all engine speeds. The distance increases from CA 110 deg. to BDC, indicating that the swirl centre moves away from the cylinder centre. After BDC, the distance decreases in the compression stroke (from CA 181 deg. to CA 360 deg.), so that the swirl centre approaches the cylinder centre again.

Table 6 shows the average value of the distance between the swirl centre and the cylinder centre during intake and compression strokes under each condition. The dimensionless distance at 1000 rpm, 1200 rpm, and 1500 rpm were 0.66, 0.65, and 0.75, respectively. From these results, since the dimensionless distance were similar, it was found that the change of the engine speed did not significantly affect the swirl centre orbit.

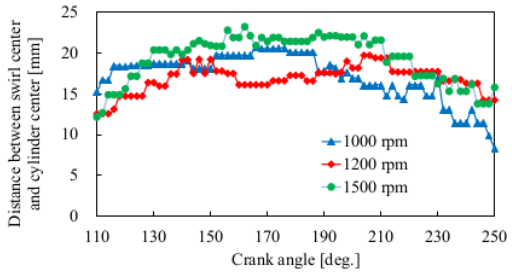

Fig. 5. Comparison of the time evolution of the distance between the swirl centre and cylinder centre under different engine speeds.

Table 6. Averaged distance between the swirl centre and the cylinder centre and dimensionless distance for each engine speed.

Engine Speed (rpm)	Distance between the swirl centre and the cylinder centre [mm]	Dimensionless distance [-]
1000	17.1	0.66
1200	16.8	0.65
1500	19.3	0.75

Figure 6 shows the plane averaged turbulent kinetic energy at each crank angle when the engine speed was varied. The figure shows that the maximum value is during the intake stroke and gradually decreases toward the compression stroke. The reason why the turbulent kinetic energy is larger during the intake stroke is considered that the air flowed strongly into the cylinder, greatly varying the instantaneous velocity field, which is also considered by Takahashi et al. [17]. On the other hand, in the compression stroke, the instantaneous velocity field became the same flow field in each cycle, and the fluctuation speed became smaller, so it is considered that the turbulent kinetic energy became smaller than in the intake stroke. Furthermore, it was confirmed that the turbulent kinetic energy increased as the engine speed increased. In this study, to evaluate the flow under various experimental conditions, the comparison for other conditions used the flow velocity under the 1000 rpm engine speed.

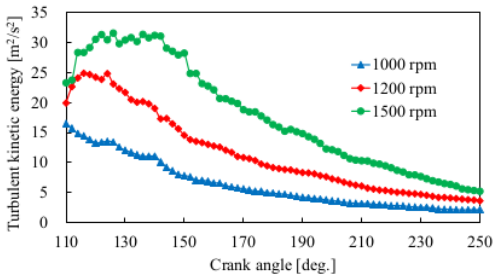

Fig. 6. Comparison of the time evolution of the turbulent kinetic energy under different engine speeds.

3.3. Comparison between different measurement planes

Figure 7 shows the ensemble-averaged velocity-vector maps for in-cylinder gas flow under 1000 rpm at z = 40 mm, 60 mm, 80 mm. The representative results at the (a) 40 mm intake, (b) 40 mm compression, (c) 60 mm intake, (d) 60 mm compression, (e) 80 mm intake, (f) 80 mm compression strokes are shown in each figure. In the measurement planes of 40 mm, 60 mm, and 80 mm, CA 90 deg. to CA 270 deg., CA 110 deg. to CA 250 deg., and CA 130 deg. to CA 230 deg. are the ranges in which PIV can be measured, respectively. For this reason, CA 130 deg. and CA 230 deg., which can be compared on all measurement planes, are the targets of the intake and compression strokes in Fig. 7, respectively.

Comparing the average velocity fields, one large vortex was observed during the intake stroke, with the swirl centre located at (x, y) = (-16.9, 1.1) and (-17.6, -0.3) at

the 60 mm and 80 mm planes, respectively. However, at the 40 mm plane, multiple vortices were observed, with the swirl centre located at (x, y) = (19.9, 0.4). Since the swirl centre identification method in this study is considered inapplicable to the case where multiple vortices are observed, it is suggested that the identification method needs to be improved. During the compression stroke, large scale vortices were confirmed at all measurement planes. However, the swirl centre locations were different. For each measurement plane, the swirl centres were (x, y) = (-7.0, -8.6), (3.9, -17.9) and (3.9, 1.3), at the 40 mm, 60 mm and 80 mm plane, respectively.

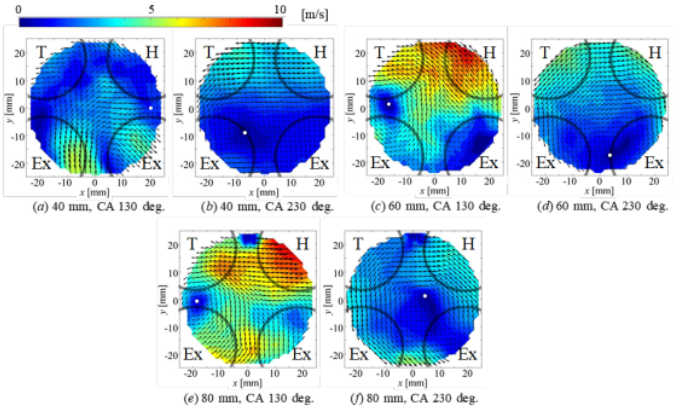

Fig. 7. Ensemble-averaged velocity-vector maps under 1000 rpm at (a) 40 mm intake, (b) 40 mm compression, (c) 60 mm intake, (d) 60 mm compression, (e) 80 mm intake, (f) 80 mm compression stroke.

Figure 8 shows the position of the swirl centres at CA 130 deg., 180 deg. and 230 deg. at each measurement plane. During each crank angle, it can be seen that the swirl centre exists at a different position when the plane changes. From the above, different flow structures could be confirmed by changing the measurement plane.

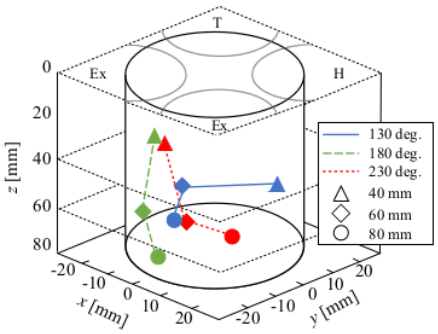

Fig. 8. Swirl centre position at each measurement plane.

3.4. Comparison between different intake port opening ratio

Figure 9 shows the ensemble-averaged velocity-vector maps for the in-cylinder gas flow under 1000 rpm at $z = 60$ mm. The intake port opening ratio comparisons were conducted under the conditions listed in Table 3, and the representative results during intake stroke at (a) Heli., (c) Tan., (e) 1/3 Heli., (g) 1/2 Heli., (i) Double and a trajectory of swirl centre in 10 deg. increments from CA 110 deg. to CA 250 deg. at (b) Heli., (d) Tan., (f) 1/3 Heli., (h) 1/2 Heli., (j) Double are shown in each figure. Figure 10 shows the distance between the swirl centre and the cylinder centre, and Table 7 shows the maximum velocities and the average values of the distance between the swirl centre and the cylinder centre during intake and compression strokes under each condition.

Comparing the average values of the maximum velocities in Table 7, 27.0 m/s for Tan. was the largest, followed by 24.1 m/s for Heli., 13.8 m/s for 1/3 Heli., 12.6 m/s for 1/2 Heli., and 10.4 m/s for Double. Thus, the flow velocity is larger under the condition when using a single port, and the tangential port only open condition is the largest. Additionally, under the condition when both ports are open, it was found that the flow velocity is larger when the opening ratio of the helical port is smaller.

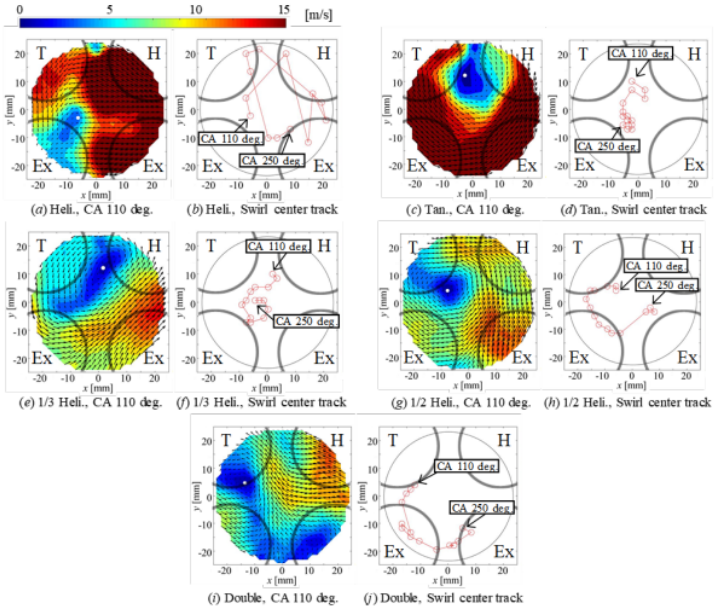

Fig. 9. Ensemble-averaged velocity-vector maps under 1000 rpm during intake stroke at (a) Heli., (c) Tan., (e) 1/3 Heli., (g) 1/2 Heli., (i) Double and a trajectory of swirl centre in 10 deg. increments from CA 110 deg. to CA 250 deg. at (b) Heli., (d) Tan., (f) 1/3 Heli., (h) 1/2 Heli., (j) Double.

Comparing the trajectory of swirl centres in Fig. 9, in the conditions (d) Tan., (f) 1/3 Heli., (h) 1/2 Heli., (j) Double, a counter-clockwise swirl centre evolution was observed, although in Heli., the swirl centres were detected at random positions. Focusing on the value of the Heli. condition in Fig. 10, there is a portion where the distance suddenly changes, and corresponding diagrams of CA 140 deg. and 216 deg. are shown in Fig. 11 as an example. In both figures, it was found that the large-scale eddies were not able to be observed. Therefore, it is considered that the reason for the sudden change in the distance between the swirl centre and cylinder centre is that it was difficult to identify the swirl centre using the calculation method of the present study due to the absence of large-scale eddies under Heli. condition. From the above, the conditions excluding Heli. (Tan., 1/3 Heli., 1/2 Heli., and Double) will be discussed.

Comparing the trajectory of swirl centres in Fig. 9, in each case, the swirl centre had a roughly counter-clockwise evolution. When the opening ratio of the helical port was increased, the distance between the swirl centre and cylinder centre became large, and the swirl centre tended to approach the cylinder centre during the compression stroke. Furthermore, comparing the values obtained by averaging the distance between the swirl centre and cylinder centre in Table 7, during the intake and compression strokes, Tan., 1/3 Heli., 1/2 Heli., and Double were 6.6 mm, 7.7 mm, 15.6 mm, and 18.1 mm, respectively. From the above, it was found that the trajectory of the swirl centre had the same tendency when the opening ratio of the helical port was varied, however, the distance between the swirl centre and cylinder centre increased when the opening area of the helical port increased.

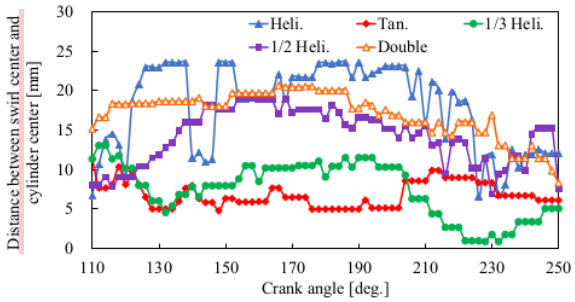

Fig. 10. Comparison of the time evolution of the distance between the swirl centre and cylinder centre at different intake port opening ratios.

Table 7. Maximum velocities and averaged distance between the swirl centre and cylinder centre for each intake port opening ratios

Parameters	Heli.	Tan.	1/3 Heli.	1/2 Heli.	Double
Maximum velocity [m/s]	24.1	27.0	13.8	12.6	10.4
Orbital radius [mm]		6.6	7.7	15.6	18.1

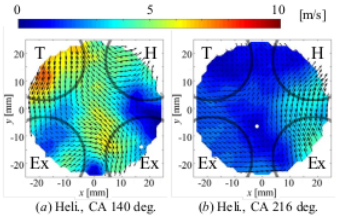

Fig. 11. Ensemble-averaged velocity-vector maps under 1000 rpm at Heli. during (a) CA 140 deg. and (b) CA 216 deg.

Figure 12 shows the swirl ratio during intake and compression strokes under each intake port opening condition. Comparing the values obtained by averaging the swirl ratio, the average swirl ratio was 5.0 for Tan. which showed the largest value, followed by 3.0 for 1/3 Heli., 2.0 for 1/2 Heli., and 1.5 for Double. From these results, it was found that the condition with the only tangential port open was the largest, and under the condition where both ports were opened, the swirl ratio became smaller by increasing the opening ratio of the helical port. This is presumably because the flow velocity decreased due to the increase in the opening ratio of the helical port.

Figure 13 shows the turbulent kinetic energy during intake and compression strokes under each intake port opening condition. Under all conditions, the graphs had similar outlines, with the maximum value during the intake stroke and a tendency to decrease toward the compression stroke. This indicates that the flow during the intake stroke has a large fluctuation and the flow during the compression stroke has less fluctuation. On the other hand, the values under each condition were different. At CA 110 deg., 31.7 m^2/s^2 for Tan. was the largest, whereas 1/3 Heli., 1/2 Heli., and double showed similar values of 19.8 m^2/s^2, 18.3 m^2/s^2, and 16.5 m^2/s^2, respectively. It is thought that the reason why the 1/3 Heli., 1/2 Heli., and double showed smaller values than the Tan. is due to the intake air from the helical port interfered with the main flow. From the above, by opening both ports, it is considered that the intake from the tangential port and the helical port interfered with each other and caused a decrease in the turbulent kinetic energy.

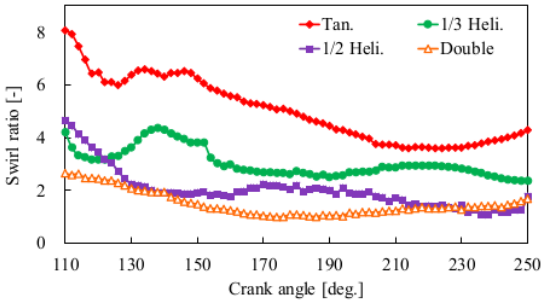

Fig. 12. Comparison of the time evolution of the swirl ratio at different intake port opening ratios.

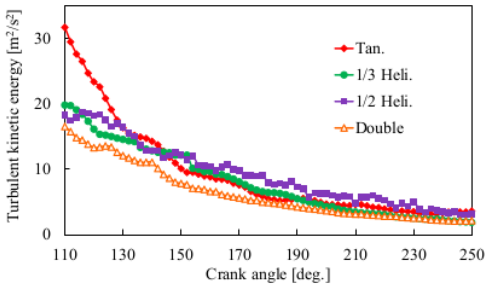

Fig. 13. Comparison of the time evolution of the turbulent kinetic energy at different intake port opening ratios.

From the above, the flow velocity was evaluated when the intake port opening ratio was changed in the 60 mm plane. In the following, the flow velocity was evaluated when the measurement plane and the intake port opening ratio were changed simultaneously. Figure 14 shows the in-cylinder average swirl ratio during intake and compression strokes at Tan., 1/3 Heli., 1/2 Heli., and Double. The swirl ratio calculated on each measurement plane is averaged to obtain an in-cylinder average swirl ratio. Considering the range of crank angles measurable by PIV for the three measurement planes, CA 130 deg. to CA 230 deg. was chosen suitable for in-cylinder swirl ratio averaging. Table 8 shows the averaged value and variance of swirl ratios for each intake port opening ratio for the 60 mm plane and the in-cylinder average. The swirl ratio obtained by the in-cylinder average was 4.8 for Tan. which showed the largest value, followed by 2.9 for 1/3 Heli., 2.1 for 1/2 Heli., and 1.2 for Double. From this result, it was found that the tangential port only open condition was the largest, and smallest under both ports open condition. The in-cylinder swirl ratio became smaller by increasing the opening ratio of the helical port. Comparing the average swirl ratios for the 60 mm plane and in-cylinder average, the values resembled at each condition. However, when comparing the variance, the results were 1.51, 0.30, 0.56, and 0.22 at the 60 mm plane, but 0.79, 0.27, 0.17, and 0.03 for the in-cylinder average for Tan., 1/3 Heli., 1/2 Heli., and Double, respectively. It was found that the variance of the in-cylinder average swirl ratio was smaller than the variance of the swirl ratio in the intake and compression strokes of a single 60 mm plane.

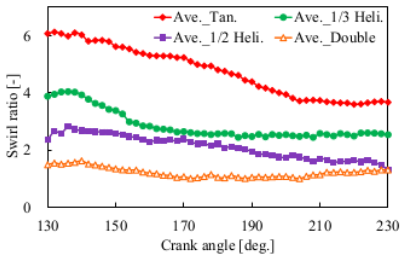

Fig. 14. Comparison of the time evolution of the in-cylinder average swirl ratio at different intake port opening ratios.

Table 8. Averaged value and variance of swirl ratios for each intake port opening ratio.

Parameters		Tan.	1/3 Heli.	1/2 Heli.	Double
Average [-]	60 mm	4.9	3.1	1.9	1.3
	Cylinder Average	4.8	2.9	2.1	1.2
Variance [-]	60 mm	1.51	0.30	0.56	0.22
	Cylinder Average	0.79	0.27	0.17	0.03

Figure 15 shows the in-cylinder average distance between the swirl centre and cylinder centre during the intake and compression strokes at Tan., 1/3 Heli., 1/2 Heli., and Double. The definition of in-cylinder average is similar to the in-cylinder average swirl ratio in Fig. 14. Table 9 shows the averaged value and variance of distances between the swirl centre and cylinder centre for each intake port opening ratio for the 60 mm plane and in-cylinder average. The distance obtained by the in-cylinder average was 16.0 mm for Double which showed the largest value, followed by 13.4 mm for 1/2 Heli., 9.0 mm for 1/3 Heli., and 6.0 mm for Tan. condition. From this result, it was found that both ports open condition was the largest, and the condition with only the tangential port open was the smallest. The distance between the swirl centre and cylinder centre became smaller by decreasing the opening ratio of the helical port. Comparing the average distances for the 60 mm plane and in-cylinder average, the value resembled at each condition. However, when comparing the variance for each condition, they were 2.60 mm^2, 12.38 mm^2, 12.36 mm^2, and 10.33 mm^2 for the 60 mm plane, but 0.66 mm^2, 4.30 mm^2, 3.24 mm^2, and 9.32 mm^2 for the in-cylinder average for Tan., 1/3 Heli., 1/2 Heli., and Double, respectively. It was found that the variance of the in-cylinder average distance between the swirl centre and cylinder centre was smaller than the variance of the distance in the intake and compression strokes of a single 60 mm plane, showing a trend similar to the swirl ratio results.

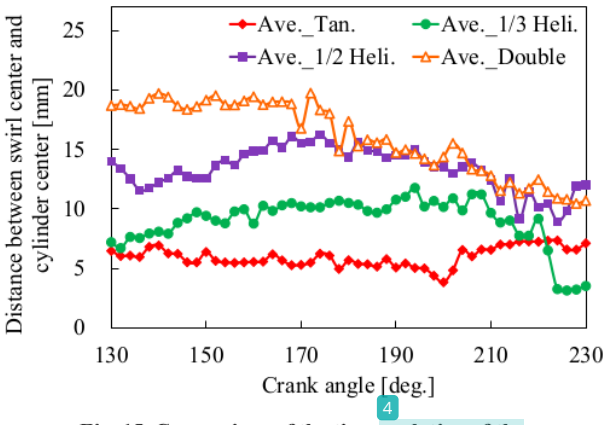

Fig. 15. Comparison of the time evolution of the in-cylinder average distance between the swirl centre and cylinder centre at different intake port opening ratios.

Table 9. Averaged value and variance of distances between the swirl centre and cylinder centre for each intake port opening ratio.

Parameters		Tan.	1/3 Heli.	1/2 Heli.	Double
Average [mm]	60 mm	6.6	7.7	15.6	18.1
	Cylinder Average	6.0	9.0	13.4	16.0
Variance [mm²]	60 mm	2.60	12.38	12.36	10.33
	Cylinder Average	0.66	4.30	3.24	9.32

Figure 16 shows the in-cylinder average turbulent kinetic energy during the intake and compression strokes at Tan., 1/3 Heli., 1/2 Heli., and Double. The definition of in-cylinder average is similar to the in-cylinder average swirl ratio in Fig. 14 and the in-cylinder average distance between the swirl centre and cylinder centre in Fig. 15. Table 10 shows the averaged value and variance of the turbulent kinetic energy for each intake port opening ratio for the 60 mm plane and in-cylinder average. The turbulent kinetic energy obtained by in-cylinder averaging was 10.4 m^2/s^2 for Tan., which showed the largest value, followed by 8.2 m^2/s^2 for 1/3 Heli., 7.8 m^2/s^2 for 1/2 Heli., and 6.0 m^2/s^2 for Double. From this result, it was found that the condition with the only tangential port open was the largest, and the smallest under both ports open condition. The in-cylinder averaged turbulent kinetic energy became smaller by increasing the opening ratio of the helical port. Comparing the average value of turbulent kinetic energy for the 60 mm plane and in-cylinder average, the value resembled at each condition, although the in-cylinder average was slightly larger. However, when comparing the variance for each condition, they were 52.40 m^4/s^4, 27.90 m^4/s^4, 23.07 m^4/s^4, and 17.26 m^4/s^4 at the 60 mm plane, but 24.64 m^4/s^4, 13.29 m^4/s^4, 8.45 m^4/s^4, and 7.37 m^4/s^4 for the in-cylinder average for Tan., 1/3 Heli., 1/2 Heli., and Double, respectively. It was found that the variance of the in-cylinder average turbulent kinetic energy was smaller than the variance of the turbulent kinetic energy in the intake and compression strokes of a single 60 mm plane, showing a trend similar to the swirl ratio results and the distance between the swirl centre and cylinder centre results. From the above, it was found that the variation for each parameter was reduced by taking the in-cylinder average in the swirl ratio, the trajectory radius, and the turbulent kinetic energy.

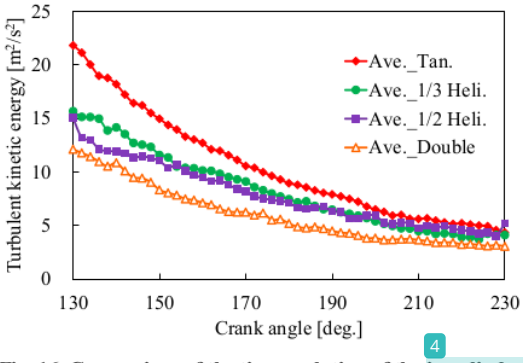

Fig. 16. Comparison of the time evolution of the in-cylinder average turbulent kinetic energy at different intake port opening ratios.

Table 10. Averaged value and variance of the turbulent kinetic energy for each intake port opening ratio.

Parameters		Tan.	1/3 Heli.	1/2 Heli.	Double
Average [m^2/s^2]	60 mm	7.5	7.4	7.8	5.7
	Cylinder Average	10.4	8.2	7.8	6.0
Variance [m^4/s^4]	60 mm	52.40	27.90	23.07	17.26
	Cylinder Average	24.64	13.29	8.45	7.37

4. Conclusions

In order to improve the fuel efficiency and exhaust gas emissions for CI engines, the swirl flow that governs the general speed and direction of the mainstream gas flow was measured. In this study, the in-cylinder swirl flow velocities in an optical single-cylinder CI engine were measured using PIV measurement under various driving conditions, engine speeds, measurement planes and intake port opening ratios. The important conclusions obtained from the present study are summarized as follows:

- The maximum velocities and the swirl centre position during intake and compression strokes obtained under motoring condition well agreed with those under firing condition. However, during the expansion and exhaust strokes, the swirl centre positions under motoring condition were far from those under the firing condition.
- Comparing the swirl centre positions during intake and compression strokes, the positions obtained under all the three engine speeds resembled. On the other hand, comparing the maximum velocities under each condition, the velocity increased as the engine speed increased. However, when comparing the non-dimensional velocity, it showed a similar value at each engine speed. From these results, it is considered that the change of the engine speed changes the velocity of the flow, without affecting the flow structure.
- The swirl centre positions during intake and compression strokes obtained at the 40 mm, 60 mm, and 80 mm planes showed different locations. From these results, different flow structures could be confirmed by changing the measurement plane.
- Comparing the swirl centre positions obtained at different intake port opening ratios, it was found under most conditions that the swirl centre showed a counter-clockwise vortex, however, the distance between the swirl centre and cylinder increased when the opening area of the helical port increased. Comparing the swirl ratios, it was found that the swirl ratio decreased when the opening ratio of the helical port increased. This is presumably because the flow velocity decreased due to the increase in the opening ratio of the helical port. Comparing the turbulent kinetic energies, it was found that all conditions had a similar tendency, but the values decreased when the opening area of the helical port increased. From these results, by opening both ports, it is considered that the intake from the tangential port and the helical port interfered with each other and caused a decrease in the turbulent kinetic energy.
- The distance between the swirl centre and cylinder centre, swirl ratio, and turbulent kinetic energy were compared when the measurement plane and the intake port opening ratio were varied simultaneously, by comparing each parameter between those of the 60 mm plane and the in-cylinder average. The tendency for the in-cylinder average in each parameter was similar to the 60 mm plane. However, when comparing the variance for each parameter, it was found

that the in-cylinder average had a smaller variance in all conditions. From the above, it was found that the variation was reduced by taking the in-cylinder average of the swirl ratio, the trajectory radius, and the turbulent kinetic energy.

Acknowledgments

This work was supported by Japan Society for the Promotion of Science, Grants-in-Aid for Scientific Research (No.16K06129 and 19K04244) and Sophia University Special Grant for Academic Research, Research in Priority Areas.

Nomenclatures

k	Turbulent kinetic energy, m^2/s^2
N	Total number of lattice points
$P_{i,j}$	Any arbitrary point
$r_{i,j}$	Position of any arbitrary point, mm
S_R	Swirl ratio
$u_{i,j}$	Velocity in x-direction, mm/s
u'	Turbulent flow velocity in x-direction, mm/s
v'	Turbulent flow velocity in y-direction, mm/s
$v_{i,j}$	Velocity in y-direction, mm/s

Greek Symbols

θ	Direction of any arbitrary point, deg.
Γ	Dimensionless scalar gamma function
ω_{engine}	Engine angular velocity, rad/s

Abbreviations

ATDC	After top dead centre
BDC	Bottom dead centre
BTDC	Before top dead centre
CA	Crank angle
CI	Combustion ignition
CO_2	Carbon dioxide
CMOS	Complementary metal-oxide semiconductor
IC	Internal Combustion
LDV	Laser doppler velocimetry
PIV	Particle image velocimetry
SI	Spark ignition
SiO_2	Silicon dioxide particles
TDC	Top dead centre

References

1. Hu, G.; Liao, S.; Zuo, Z.; Wang, K.; and Zhu, Z. (2018). Kinetic effects of methanol addition on the formation and consumption of formaldehyde and

benzene in premixed n-heptane/air flames. *Journal of Energy Resources Technology*, 140(7), 072205.

2. Anggono, W.; Hayakawa, A.; Okafor, E.C.; Gotama, G.J.; and Wongso, S. (2020). Laminar burning velocity and Markstein length of CH_4/CO_2/Air premixed flames at various equivalence ratios and CO_2 concentrations under elevated pressure. *Combustion Science and Technology*.
3. Elango, T.; and Senthilkumar, T. (2011). Performance and emission characteristics of CI engine fuelled with non edible vegetable oil and diesel blends. *Journal of Engineering Science and Technology* (*JESTEC*), 6(2), 240-250.
4. Mohamad Shafie, N.A.; and Muhamad Said, M.F. (2017). Cold flow analysis on internal combustion engine with different piston bowl configurations. *Journal of Engineering Science and Technology* (*JESTEC*), 12(4), 1048-1066.
5. Anggono, W.; Ikoma, W.; Chen, H.; Liu, Z.; Ichiyanagi, M.; Suzuki, T.; and Gotama, G.J. (2019). Investigation of intake pressure and fuel injection timing effect on performance characteristics of diesel engine. *IOP Conf. Series: Earth and Environmental Science,* 257(012037).
6. Boopathi, D.; Sonthalia, A.; and Devanand, S. (2017). Experimental investigations on the effect of hydrogen induction on performance and emission behaviour of a single cylinder diesel engine fuelled with palm oil methyl ester and its blend with diesel. *Journal of Engineering Science and Technology (JESTEC),* 12(7), 1972-1987.
7. Xu, L.; Bai, X.; Li, Y.; Treacy, M.; Li, C.; Tunestål, P.; Tunér, M.; and Lu, X. (2020). Effect of piston bowl geometry and compression ratio on in-cylinder combustion and engine performance in a gasoline direct-injection compression ignition engine under different injection conditions. *Applied Energy*, 280, 115920.
8. Yilmaz, E.; Ichiyanagi, M.; and Suzuki, T. (2019). Development of heat transfer model at intake system of IC engine with consideration of backflow gas effect. *International Journal of Automotive Technology*, 20(5), 1065-1071.
9. Takahashi, D.; Nakata, K.; Yoshihara, Y.; and Omura, T. (2016). Combustion Development to Realize High Thermal Efficiency Engines. *SAE International Journal of Engines*, 9(3), 1486-1493
10. Tyagi, R.K.; Sharma, S.K.; Chandra, A.; Maheshwari, S.; and Goyal, P. (2015). Improved intake manifold design for IC engine emission control. *Journal of Engineering Science and Technology (JESTEC)*, 10(9), 1188-1202.
11. Heim, D.; and Ghandhi, J. (2011). A detailed study of in-cylinder flow and turbulence using PIV. *SAE International Journal of Engines,* 4(1), 1642-1668.
12. Kim, Y.; Han, Y.; and Lee, K. (2014). A Study on the Effects of the Intake Port Configurations on the Swirl Flow Generated in a Small D.I. Diesel Engine. *Journal of Thermal Science*, 23(3), 297-306.
13. Okura, Y.; Higuchi, K.; Urata, Y.; Someya, S.; and Tanahashi, M. (2013). Measurement of in-cylinder turbulence in an internal combustion engine using high speed particle image velocimetry. *Transactions of the Japan Society of Mechanical Engineers Series B*, 79(806), 2193-2206.

14. Garcia-Oliver, J.; Garcia, A.; Gil, A.; and Pachano, L. (2017). Study of Air Flow Interaction with Pilot Injections in a Diesel Engine by Means of PIV Measurement. *SAE International Journal of Engines,* 10(3), 740-751.
15. Ichiyanagi, M.; Ndizeye, G.; Sawamura, Y.; Saito, R.; Takahashi, K.; Otsubo, K.; Chen, H.; and Takashi, S. (2019). Improvement of on-board in-cylinder gas flow model and wall heat transfer prediction model for CI engines using CFD analysis and PIV measurements under motoring and firing conditions. *SAE Technical Paper,* 2019-32-0542.
16. Zha, K.; Bush, S.; Miles, P.; Wijeyakulasuriya, S.; Mitra, S.; and Senecal, P.K. (2015). Characterization of flow asymmetry during the compression stroke using swirl plane PIV in a light-duty optical diesel engine with the re-entrant piston bowl geometry. *SAE International Journal of Engines*, 8(4), 1837-1855.
17. Zhuang, H.; and Hung, D.L.S. (2016). Characterization of the effect of intake air swirl motion on time-resolved in-cylinder flow field using quadruple proper orthogonal decomposition. *Energy Conversion and Management*, 108, 366-376.

16_5_01

ORIGINALITY REPORT

11%	5%	8%	0%
SIMILARITY INDEX	INTERNET SOURCES	PUBLICATIONS	STUDENT PAPERS

PRIMARY SOURCES

1	Daiki Goto, Yuji Sawamura, Gerard Ndizeye, Mitsuhisa Ichiyanagi, Takashi Suzuki. "ディーゼル機関におけるPIV測定による筒内スワール流の評価", The Proceedings of the Thermal Engineering Conference, 2018 Publication	3%
2	jestec.taylors.edu.my Internet Source	2%
3	Saad ALJARF, Hardeep SINGH, Gerard NDIZEYE, Mitsuhisa ICHIYANAGI, Takashi SUZUKI. "Effect of dual air inlet port of 4-valve CI engine on the swirl flow generated at bottom region of the cylinder using PIV technique", Mechanical Engineering Journal, 2021 Publication	2%
4	A-F M Mahrous, M L Wyszynski, T Wilson, H-M Xu. "Computational fluid dynamics simulation of in-cylinder flows in a motored homogeneous charge compression ignition engine cylinder with variable negative valve	1%

overlapping", Proceedings of the Institution of Mechanical Engineers, Part D: Journal of Automobile Engineering, 2007
Publication

5	G. Cantore, S. Fontanesi, E. Mattarelli, G. M. Bianchi. "A Methodology for In-Cylinder Flow Field Evaluation in a Low Stroke-to-Bore SI Engine", SAE International, 2002 Publication	1 %
6	repository.petra.ac.id Internet Source	1 %
7	Submitted to Sophia University Student Paper	<1 %
8	livrepository.liverpool.ac.uk Internet Source	<1 %
9	www.mdpi.com Internet Source	<1 %
10	Bambang Wahono, Ardhika Setiawan, Ocktaeck Lim. "Effect of the intake port flow direction on the stability and characteristics of the in-cylinder flow field of a small motorcycle engine", Applied Energy, 2021 Publication	<1 %

Exclude quotes On Exclude matches < 30 words

Exclude bibliography On